ADVANCED ENGINEERING MATERIALS
www.aem-journal.com

Influence of Gas Pressure and Blowing Agent Content on the Formation of Aluminum Alloy Foam

Francisco García-Moreno and John Banhart*

Apart from density and alloy composition, the structure of solid metallic foams determines their mechanical performance. Herein, the effect of ambient pressure on the foaming behavior of AlSi6Cu4 precursors is studied. In situ X-ray radioscopy is applied while foaming in a furnace chamber pressurized up to 40 bar. The content of the blowing agent (TiH_2) is varied for each of the pressures chosen. The foam density and morphology are analyzed quantitatively using time-resolved X-ray radioscopy sequences and postsolidification X-ray tomography data. The optimal content of blowing agent as well as the pore sizes and distributions is found to depend strongly on the ambient pressure. At high pressures very small, round, and uniformly distributed pores are formed and crack formation is avoided during the gas nucleation stage, which helps to prevent structural defects. Adjusting the ambient pressure allows for better control of the foam structure and density, which is relevant for commercial production and application.

1. Introduction

Metal foaming following the powder metallurgical (PM) route is nowadays one of the most promising methods for industrial production.[1–3] Serial production of complex parts foamed in a mould is now reality.[3] Although foam quality has been increasing step by step in the past decades, the still existing reliability problems during production are hindering an expansion of the market for metal foam components. In addition to the foam density and alloy composition, the foam structure is the most important attribute governing quality, which, however, is difficult to control. Apart from cost issues, reproducibility of the foam structure, and consequently foam properties, is the most urgent challenge. Several aspects and processing parameters such as the precursor compaction conditions,[4] alloy composition,[5–8] type or pretreatment of the blowing agent[9,10] and its content,[10] foaming temperature profile,[5,11] and gas nucleation[12,13] play a very important role in the foaming process as the quality of the resulting structure is very sensitive to variations of one or more of the parameters.[5,14,15] Till date, the influence of the gas pressure surrounding an expanding foam has hardly been studied, possibly because of the complexity of the equipment required.[15–17]

Constant atmospheric pressure is usually applied during metal foaming for reasons of simplicity. Some previous works have already shown that the pore size, degree of volume expansion, and structure of Al-based foams depend on the pressure during foaming.[15,16,18–20] In these studies, a fixed content of blowing agent driving foam expansion (usually 0.5 wt% TiH_2) was used, which is a standard content that ensures best foaming under normal atmospheric gas pressure.[21] Foaming without any blowing agent is also possible by manipulating the pressure during the process.[20] A similar method is commercially applied for foaming polymers, in which CO_2 is dissolved under pressure and gas nucleation and foaming are induced by pressure release.[22]

In this work, we present a systematic study of the influence of ambient pressure in the range 1–40 bar during foaming of an AlSi6Cu4 alloy on the pore size, density, and structure of the corresponding foam. Hereby we vary the content of blowing agent between 0.5 and 10 wt% TiH_2 with the objective of optimizing foam expansion and maintaining a uniform pore structure.

2. Experimental Section

2.1. Precursor Preparation

Elemental powders of air-atomized aluminum (Alpoco Ltd., Sutton Coldfield, UK, 99.7% purity, $D_{50} = 38\ \mu m$), silicon (Wacker Chemie, Munich, Germany, 99.5% purity, $D_{50} = 26\ \mu m$), and copper (Chempur GmbH, Karlsruhe, Germany, 99.7% purity, $D_{50} = 33\ \mu m$) were used for precursor production. TiH_2 powder (Chemetall GmbH, Frankfurt am Main, Germany, 98.8% pure, $D_{50} = 14\ \mu m$) was added as a blowing agent. The powders were mixed in air for 30 min in a tumbling mixer. Cylindrical precursors (20 g, 36 mm diameter, 8 mm height) of AlSi6Cu4 (in wt%) with an addition of 0.5, 1, 2.5, 5, and 10 wt% TiH_2 was prepared by uniaxial hot compaction (300 MPa, 400 °C, 5 min) of the elemental powders following the standard PM route.[1] Rectangular samples

Dr. F. García-Moreno, Prof. J. Banhart
Institute of Applied Materials
Helmholtz-Zentrum Berlin
Hahn-Meitner Platz 1, 14109 Berlin, Germany
E-mail: garcia-moreno@helmholtz-berlin.de

Dr. F. García-Moreno, Prof. J. Banhart
Institute of Materials Science and Technology
Technische Universität Berlin
Hardenbergstrasse 36, 10623 Berlin, Germany

The ORCID identification number(s) for the author(s) of this article can be found under https://doi.org/10.1002/adem.202100242.

DOI: 10.1002/adem.202100242

of dimensions 20 mm × 10 mm × 3 mm were cut out of the precursors for X-ray radioscopic foaming analysis.

2.2. Foaming Method

For the in situ analysis of the foaming behavior under gas pressure, a novel X-ray transparent pressure chamber was designed and built (see **Figure 1**). This furnace is composed of a stainless steel vacuum chamber, which can be operated from 10^{-3} mbar to 40 bar pressure. Herein, Ar was used as a cover gas to avoid oxidation effects. Two AlMg1 (in wt%) windows, each 2 mm thick and 80 mm in diameter, allowed for good transmission of X-rays and in-situ X-ray observation of the foaming process. Foaming took place on a ceramic heating plate of 75 mm × 45 mm × 4.3 mm size (Bach-RC, Berlin, Germany, 230 V, ≈1000 W) located inside the pressure chamber. Two thermocouples allowed for recording temperature profiles: The one situated inside the sample was used only for reference measurements, and the one inside the heating plate was close to the sample bottom and connected to a CAL 3300 PID temperature controller (CAL Controls, Hertfordshire, UK). The latter allows for a precise adjustment of the foaming temperature profile (640 °C set temperature with a heating rate of 16.7 K s^{-1}), while the former provides the absolute temperature of the sample and was used only for the purpose of calibration.

2.3. Foam Analysis

The foaming behavior was studied in situ with an X-ray radioscopy setup composed of a microfocus X-ray tube operated at 100 kV voltage, 100 µA current, and 5 µm spot size, and a 120 mm × 120 mm C7942CA flat panel detector (50 µm pixel size, 2240 × 2368 pixel), both from Hamamatsu Photonics, Hamamatsu, Japan, described in detail elsewhere.[23] A magnification of 4 was applied, leading to an effective pixel size of 12.5 µm in the radiograms. High-resolution images of the cellular structure evolution were recorded with 1 Hz throughout the foaming process. Foam expansion evolution A_f/A_0 in terms of projected foam area A_f related to the projected precursor area A_0 was calculated quantitatively from the radioscopic image sequence as explained in the literature.[23] The volume of the foam V_f corresponds to the sum of the precursor volume V_0 and the gas volume inside the foam V_G. For small square samples, surface tension rounds off the contour of the precursor so that the resulting foam is eventually not cuboid but roughly spherical. For such a case we commonly approximate the corresponding volume expansion V_f/V_0 of freely expanding liquid metal foams by[20]

$$\frac{V_f}{V_0} = \left(\frac{A_f}{A_0}\right)^{\frac{3}{2}} \tag{1}$$

In the current case, the precursor sample was not a square but a rectangle with an aspect ratio of 2:1 and the resulting foam was more in the shape of a bread loaf. For an infinitely long sample, lateral expansion can be neglected and the foam would be best approximated by a cylinder and the power law in Equation (1) would change from $\frac{3}{2}$ to 3, but the current case is closer to that described by $\frac{3}{2}$ because one can think of two squares foamed next to each other and each one shows full lateral expansion on one side and a somewhat modified situation where the two foams touch. Equation (1) is therefore used in the following.

The X-ray setup shown in Figure 1 was also used for computer tomography of the solidified foams by replacing the furnace by a rotation stage 408-X2W1 from Huber, Berching, Germany. The samples were rotated over 360°, during which 1000 images were recorded every angular step of 0.36°. This took around 1 h. In a second step, the 1000 projections were mathematically reconstructed to a 3D volume[24] using the commercial software Octopus. The geometrical magnification of 5.7 applied resulted in an effective voxel size of the reconstructed volume of 8.8 µm. Quantitative analyses of foam density, pore size distribution, and mean pore diameter were performed with the commercial software Avizo Fire.

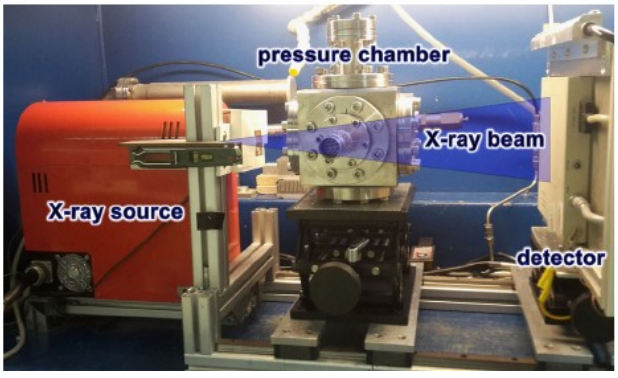

Figure 1. Experimental setup consisting of a microfocus X-ray source, a pressure foaming chamber with a heater inside and two thin Al foil windows to let the X-ray beam pass, and a flat panel detector.

3. Results

In a preliminary experiment it was found that for 1 bar ambient pressure and 640 °C foaming temperature, foam full expansion was reached after ≈140 s. This time was set as the time when the heater power was switched off in all the experiments. X-ray radiograms of solidified foam structures as they appeared after the end of expansion (after 240 s) were extracted from the radioscopy sequences measured in situ and are shown in **Figure 2**. They reveal differences in the foaming behavior and structure development depending on the ambient pressure applied as expected from previous work.[20] Figure 2 also shows the influence of the blowing agent content on foaming for different pressures. Although each parameter could be further optimized in terms of compaction conditions, foaming temperature, heating rate, etc., in an iterative manner, all the remaining process parameters were kept constant to allow us to focus on the relationship between ambient pressure and blowing agent content, and to limit the number of experiments to a manageable number.

3.1. Foam Expansion and Morphology

For 0.5 wt% TiH_2 content, foam expansion was highest at 1 bar and decreased together with the mean pore size as pressure increased. Simultaneously, there was an additional increase of pore uniformity as shown in Figure 2. A few cracks in the precursors with 0.5 wt% TiH_2 were observed during foaming under 1 and

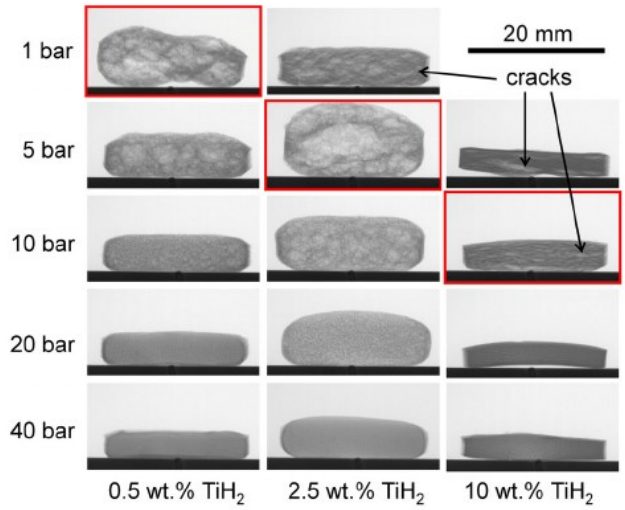

Figure 2. X-ray radiographs of AlSi6Cu4 samples foamed at 640 °C in an argon gas atmosphere pressurized to 1, 5, 10, 20, and 40 bar. The state after $t = 240$ s from the beginning of heating is shown. Samples contain 0.5, 2.5, or 10 wt% TiH_2. The foam structure and projected area expansion can be observed. The red boxes mark conditions of maximum expansion for the three different TiH_2 contents, black arrows cracks in the solid foams.

5 bar, but not for higher pressures. When using 2.5 wt% TiH_2, some cracks were found until 10 bar pressure and the highest end expansion was achieved at 5 bar, but the resulting foam structure was not uniform and some large pores were observed evolving from the former cracks in the precursor (see Video S1, Supporting Information). For 10 bar pressure and higher, spherical and very small uniformly distributed pores could be obtained for every condition. For 10 wt% TiH_2, the maximum expansion was shifted to 10 bar pressure, but the absolute area expansion compared to 0.5 and 2.5 wt% TiH_2 content was visibly reduced and crack-like elongated pores remained in the solid foam as shown in Figure 2. In general, we obtain less expansion, smaller pores, and more uniform structures for higher pressures. The higher the pressure, the higher is the blowing agent content required for a given maximum expansion (pictures marked by a red frame in Figure 2).

3.2. Expansion Profiles

The quantitative analysis of the volume expansion evolution during foaming extracted from the X-ray radioscopic sequences and expressed by the increase of the projected foam area is shown in **Figure 3** for different pressures and exemplarily for a blowing agent content of 0.5 wt% TiH_2. Foaming started at 30–40 s for all conditions and followed typical expansion profiles as known from the literature.[15] All expansion profiles feature fast growth in the beginning, with several shoulders pointing at a varying growth rate caused by a temperature-dependent but nonlinear liquid fraction evolution[7] and gas release of the blowing agent.[25] For 10 and 20 bar pressure, a small maximum was observed. All the samples showed a horizontal expansion plateau until the heater was switched off. The liquid foams then started to shrink and showed the effect of solidification expansion[26] shortly before the final solidification took place at 190 s and 425 °C.

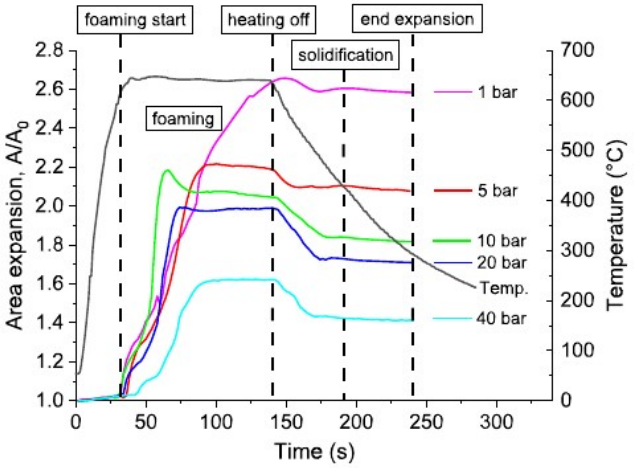

Figure 3. Colored: area expansion curves for AlSi6Cu4 + 0.5 wt% TiH_2 samples foamed at 640 °C under 1, 5, 10, 20, and 40 bar Ar; black: exemplary temperature profile.

3.3. Pressure Dependence of Foam Expansion

The resulting end expansion at 240 s, when the solid samples reached ≈300 °C, is shown in **Figure 4** as a function of applied gas pressure for different contents of TiH_2. For 0.5 and 1 wt% TiH_2, expansion decreases with pressure. For blowing agent contents >1 wt% we observe a maximum located at 5 bar for 2.5 wt% TiH_2, increasing to 20 bar for 5 wt% TiH_2, but decreasing again to 10 bar for 10 wt% TiH_2.

3.4. Pressure Dependence of Pore Size and Density

2D slices extracted from the tomographic volumes show the pore structures of solidified foams produced with different contents of blowing agent under 40 bar pressure (see **Figure 5**a). Foams

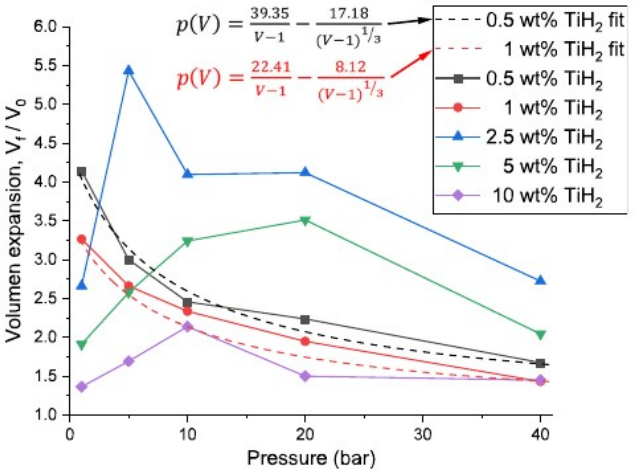

Figure 4. Final (= after 240 s) volume expansion as a function of argon pressure for different contents of TiH_2. The dashed black and red lines show the fit of the curves according to Equation (2) for 0.5 and 1 wt% TiH_2, respectively.

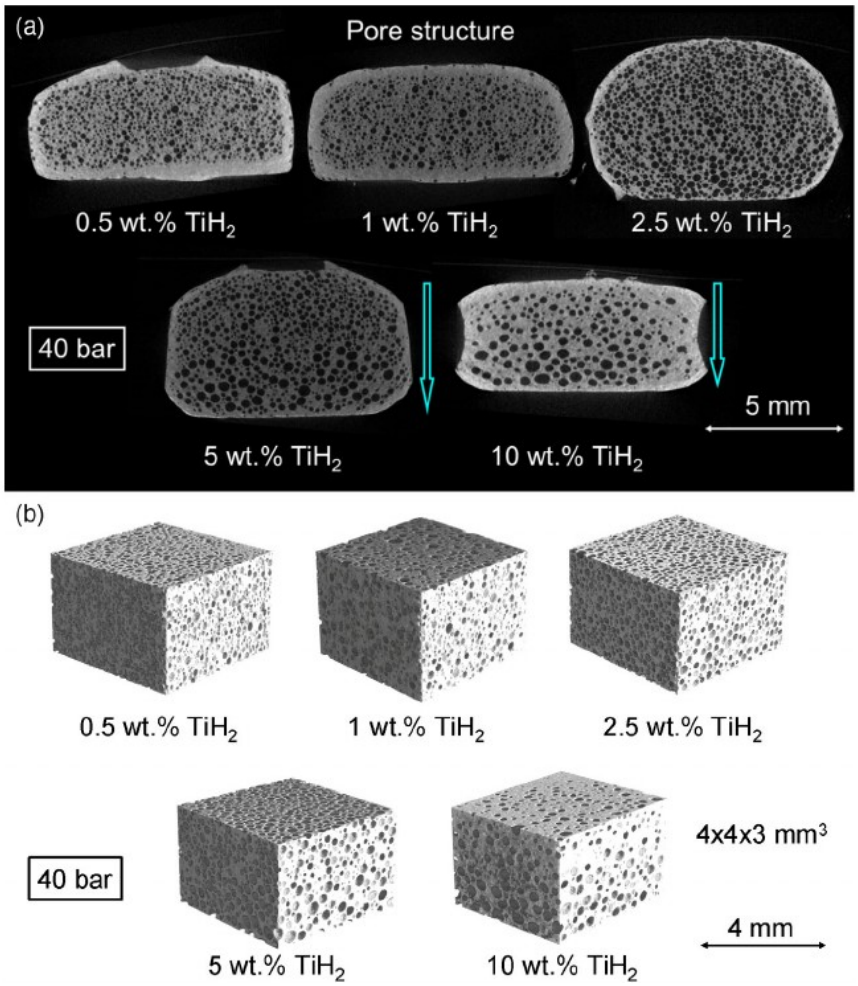

Figure 5. a) 2D slices and b) rendered images of 3D tomographic reconstructions of the pore structure of AlSi6Cu4 samples foamed with 0.5, 1, 2.5, 5, and 10 wt% TiH_2 under a 40 bar argon atmosphere. The cyan arrows show the pore size gradient from top to bottom, especially visible in samples with high TiH_2 content.

made at this high pressure exhibit neither cracks nor big pores or defects, even when using 10 wt% TiH_2 (see also Figure 2), but relatively spherical pores. We observe a slight pore size increase with increasing TiH_2 content as well as a pore size gradient with increasing pore size from the top to the bottom in the samples containing $\geq$5 wt% TiH_2 (as indicated by arrows in Figure 5a). Furthermore, an $\approx$0.5 mm thick dense outer skin is visible in all the samples.

Representative tomograms of dimensions 4 mm × 4 mm × 3 mm are shown in 3D-rendered images (see Figure 5b). They demonstrate that the structure is quite uniform and no cracks can be found in any direction. Quantitative image analyses of the reconstructed 3D volumes can deliver further detailed information. For this purpose, the mean pore size and the relative density of the samples were plotted against the content of TiH_2 in **Figure 6** for 40 bar gas pressure. The mean pore size diameter increases with the content of TiH_2, but there is a pronounced minimum of the relative foam density at 2.5 wt% TiH_2 (see Video S2, Supporting Information). The pore number density versus the content of TiH_2 for foaming under 40 bar pressure shows a maximum at 2.5 wt% TiH_2 (see **Figure 7**). For this pressure and content of TiH_2, we also find a maximum foam volume expansion (see Figure 4) and a minimum in the mean pore size (see Figure 6). The corresponding normalized pore size distribution (see **Figure 8**) is wider the larger the TiH_2 content is.

4. Discussion

4.1. Process Parameters

The optimization of foam quality in terms of end expansion and cell morphology for different blowing agent contents has been studied in the past for aluminum-based foams of different alloy systems, e.g., AlSiX,[5,8,21] AlSiXCuY,[8] and AlSiXMgY,[27] but almost exclusively by foaming under ambient atmospheric conditions. Foaming in normal atmosphere is of course the cheapest and most simple way of foam production, but not necessarily the best in terms of structural quality of the solid foams obtained. As already observed in Figure 2, the ambient pressure is a very

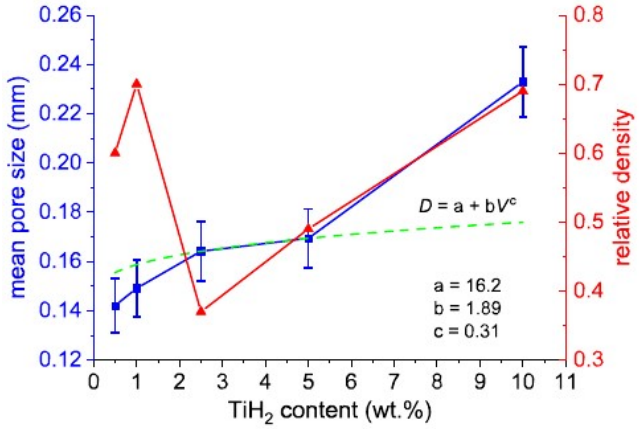

Figure 6. Pore size diameter (blue squares) in dependence of the content of TiH_2 in the precursors and the corresponding foam relative density (red triangles) for samples foamed under 40 bar. The dashed green curve represents a fit of the mean pore size according to Equation (3).

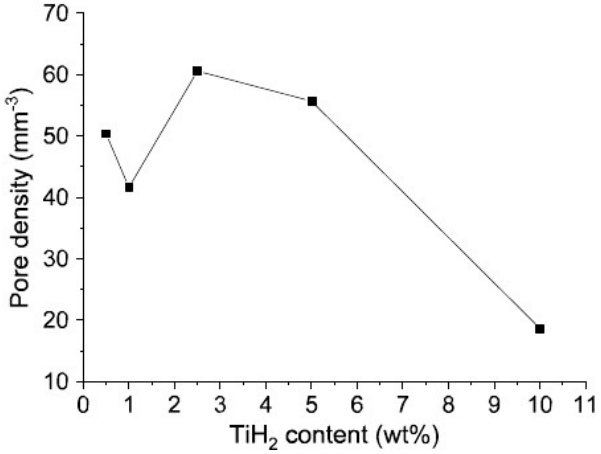

Figure 7. Pore density as a function of TiH_2 content in the precursors for samples foamed under 40 bar gas pressure.

important production parameter as it is the case in the production of polymeric foams,[22] although for such foams gas dissolution plays a major role.

4.2. Foam Expansion

When foaming aluminum alloys under ambient conditions following the PM route, a blowing agent content of 0.5 wt% TiH_2 is considered a good compromise for obtaining a pronounced expansion and high foam quality.[28] In the current work, foam expansion was found to depend strongly on the ambient pressure and on the content of blowing agent used. Figure 2 shows different maximum expansions for different TiH_2 contents in the alloy AlSi6Cu4 depending on pressure. The reason is that for a given ambient pressure, a too low content of TiH_2 leads to a low final foam expansion due to the lack of available gas. A shift of the maximum expansion to values <0.5 wt% TiH_2 can be expected for pressures <1 bar, similarly to what has been previously shown for pure Al foams foamed under 10^{-2} bar pressure.[15] In contrast, too much TiH_2 gives rise to cracks in the precursor prior to the onset of foaming because of excessive internal gas pressure building up upon heating, which cannot be counteracted by the yield strength of the compact. As a consequence we observe cracks in the precursors, which lead to gas losses to the environment and, at a later stage, when the temperature further increases and the alloy foams completely, to large bubbles, lower expansion values, and nonuniform solid foam structures. Such structures are prone to collapse in the liquid state[15] and are detrimental for the mechanical properties of the corresponding solid foams.[29,30]

For a fixed TiH_2 content of e.g. 0.5 wt%, as shown in Figure 3a, a higher ambient pressure causes a lower maximum foam expansion. This is because the equilibrium between gas pressure in the bubbles and the ambient pressure is reached earlier, thus hindering the bubbles from further increasing their volume as already shown by Körner et al. for AlSi10Mg foams.[18] This applies to not only 0.5 wt% but also 1 wt% TiH_2, as shown in Figure 4 for the pressure range studied. Volume expansion is proportional to foam porosity, i.e., to the gas volume in the foam, which should be inversely proportional to the internal gas pressure p_{int} according to ideal gas law. At the equilibrium point of foam expansion, p_{int} is counteracted by the sum of the ambient pressure $p_{amb}$and the Laplace pressure in the bubbles simplified to a unique radius r leading to

$$p_{amb}(V) = \frac{\alpha}{V_f - 1} - \frac{\beta}{(V_f - 1)^{\frac{1}{3}}} \quad (2)$$

with α and β as the fitting parameters for the ideal gas and Laplace pressure components, respectively. This function represents the data curves corresponding to 0.5 and 1 wt% TiH_2 (see Figure 4), but for higher TiH_2 contents it is no longer valid. And, in fact, considering former results at low pressure, this relationship also does not apply.[15]

Therefore, in addition to ambient pressure, other aspects such as temperature-dependent gas production kinetics,[25] crack formation,[31] gas losses,[20,26] and liquid foam internal structural stability[32] influence expansion too and lead to an ideal, pressure-dependent content of TiH_2 for each applied external pressure that does not follow from the aforementioned simple equation.

In a foamable aluminum precursor, hydrogen is mainly delivered by the blowing agent (TiH_2 here) and by adsorbates on the metal powders, and therefore all potentially available gas at 660 °C has a volume of around 30 times the volume of the precursor by using 0.5 wt% TiH_2.[20] When using, e.g., 2.5 wt% TiH_2 under 1 bar we should obtain five times more gas volume, corresponding to 150 times the precursor volume. Under 40 bar pressure this volume should be reduced to a final volume expansion of 4.75 (150/40 + 1). Figure 4 shows that for this condition the final foam volume expansion is around 2.83. This means that ≈60% of the total available gas is used for foaming, which is much more than the usual ≈25% under normal (1 bar) pressure.[20] We can conclude that the gas yield for foaming is larger at higher pressures because of the reduction in gas losses.

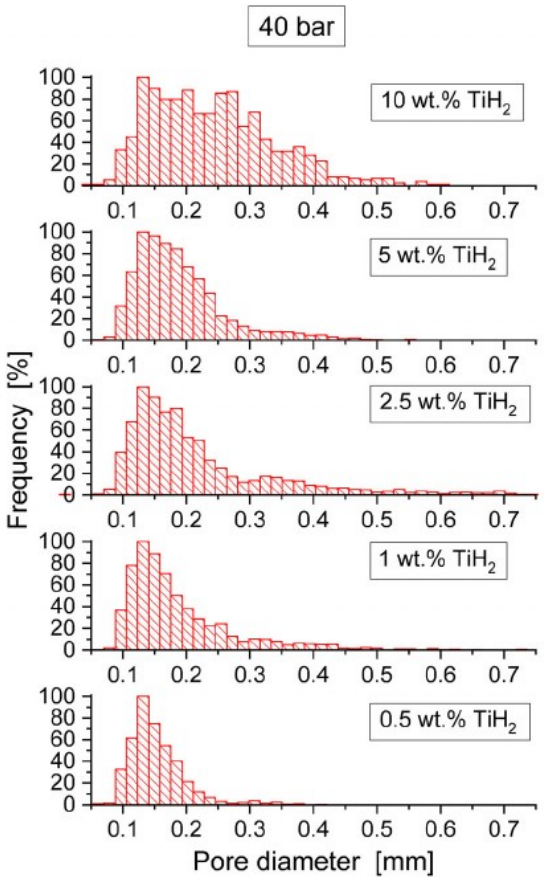

Figure 8. Normalized pore size distribution of samples with different TiH_2 contents foamed under 40 bar pressure (see Figure 5 and 6).

4.3. Foam Morphology

A pronounced foam expansion is important as it leads to a low relative density of the material, but a uniform structure is also required to obtain a corresponding good mechanical performance, e.g., high strength and modulus values, and good reproducibility of properties.[29] The final structure of a solid foam is first influenced by the distribution of bubble nucleation sites,[13] and then by the uniformity of bubble inflation and their uniform distribution throughout foaming,[33] which are directly influenced by the presence of TiH_2 particles. The structure, in turn, depends on coalescence in the course of foaming,[34] i.e., on the internal structural stability of the foam.[32] At least one or several of these processes must be influenced by an external pressure as the dependence of the final foam structure on pressure shows.

For the nucleation of a bubble, its internal pressure has to be at least as high as the ambient pressure plus the Laplace pressure as given by Equation (2). On increasing the ambient pressure, the minimal nucleation pressure has to increase, too. As shown in Figure 2 and 5, bubble nucleation and expansion occur even in an atmosphere pressurized to 40 bar. This demonstrates that the internal gas pressure of the nucleating bubbles can exceed at least 40 bar.

The formation of an outer bulk skin around the samples (see Figure 5a), especially at high pressures, can be explained by the way the blowing gas (hydrogen) is generated, diffuses, and nucleates. Hydrogen originates first from adsorbates at the locations of former powder particle surfaces[13,20] and is provided later by decomposing TiH_2 particles. Diffusion of the cover gas (argon) can be neglected. Hydrogen generated very close to the sample surfaces preferentially diffuses out to the surrounding instead of nucleating in new gas bubbles as the hydrogen located more in the interior of the sample does. The influence of a gas atmosphere on outdiffusion has been shown in the literature.[35] A hydrogen concentration gradient to the surrounding is the consequence,[26] leading to a nucleation-free layer around the sample.

4.4. Pore Size and Foam Density

Körner et al. demonstrated that the mean pore size and the level of porosity of metal foams decrease with the ambient pressure increasing from 0.5 to 2.8 bar, while leaving the TiH_2 level constant.[18] At a constant pressure and according to the ideal gas law, the gas volume in the pores, assuming a constant pore number density, should be proportional to the cubed pore mean diameter D, and therefore

$$D \sim V^{1/3} \tag{3}$$

When keeping the ambient pressure constant, e.g., at 40 bar as shown in Figure 5 and 6, the mean pore size increases with increasing content of TiH_2, i.e., with the hydrogen concentration. The relationship suggested in Equation (3) seems to be valid up to a content of TiH_2 of 5 wt% as shown by a green dashed line in Figure 6, where the pore density ranges from 40 to 60 mm^{-3}, but cannot be verified for higher TiH_2 contents as, e.g., the pore density decreases to $\approx$19 mm^{-3} for 10 wt% TiH_2 (see Figure 7). There is also no clear relationship between relative foam density and content of TiH_2 as Figure 6 shows. All these aspects demonstrate that the influences of ambient pressure reach beyond simple gas-phase properties, such as the nucleation rate, gas losses, and crack formation, as stated previously.

With an increasing content of gas available in the sample at a constant ambient pressure, an increased level of bubble coalescence is observed, reflected in a reduced absolute number of pores and an increase of larger ones, as well as on a wider pore size distribution as shown in Figure 8. The latter can be attributed to the larger coalescence rate induced by a higher blowing agent content.[32,34]

The pore size gradient from the top to the bottom observed in Figure 5a may be just an artifact of the experimental setup applied as the samples are placed on top of a heating plate and due to the good thermal conductivity of the aluminum-based samples the temperature at the bottom is very similar to that at the top under 1 bar ambient pressure, but cooling the upper side of the samples plays a greater role under 40 bar pressure due to the increased thermal conductivity of the atmosphere and could therefore cause a gradient.

4.5. Blowing Agent Optimization

Increasing the ambient pressure avoids crack formation and allows for increasing TiH_2 additions, while leading to large

volume expansion and a more uniform pore structure. Increasing pressure, however, is favorable only to a limited extent. Too high pressures lead to uniform structures but with a largely reduced expansion, i.e., with higher relative density, as the bubbles cannot sufficiently grow more due to the lack of blowing gas.

Metal foaming under elevated gas pressure also allows for better control of the desired foam structure and density, which could be relevant for commercial foam production, e.g., when foaming components in a closed mold. Such molds could be directly pressurized, similarly to high-pressure die casting.[36]

5. Conclusion

Metal foam expansion, pore size, and structural uniformity strongly depend on both the ambient atmospheric pressure and the blowing agent content: 1) Elevated ambient pressures up to 40 bar during foaming positively influence pore nucleation and lead to smaller, more homogeneously distributed pores and to more uniform foam structures than normal atmospheric pressure, but at the cost of a higher foam density. 2) The higher is the pressure, the fewer cracks form and gas losses during heating are reduced, thus increasing the gas yield. 3) There is an optimal content of blowing agent to reach maximal expansion, i.e., the lowest relative density, for a given ambient pressure. For example, for 1 and 40 bar the optimal contents of TiH_2 in the AlSi6Cu alloy were found to be 0.5 and 2.5 wt% TiH_2, respectively. 4) At a given ambient pressure, insufficient TiH_2 causes too low expansion, but too much TiH_2 leads to cracks, bubble coalescence, and gas losses caused by too high internal gas pressure and eventually to fewer pores varying more in size.

Supporting Information

Supporting Information is available from the Wiley Online Library or from the author.

Acknowledgements

The authors gratefully acknowledge funding by the European Space Agency ESA (Project "μg-Foam," AO–99–075) and by the German Research Foundation DFG (Project "sub-mm bubbles," BA 1170/35-1 and GA 1304/5-1).

Open access funding enabled and organized by Projekt DEAL.

Conflict of Interest

The authors declare no conflict of interest.

Data Availability Statement

Research data are not shared.

Keywords

ambient pressure, blowing agents, metal foams, tomography, X-ray radioscopy

Received: February 26, 2021
Revised: May 7, 2021
Published online:

[1] J. Banhart, *JOM* **2000**, *52*, 22.
[2] a) J. Banhart, H.-W. Seeliger, *Adv. Eng. Mater.* **2012**, *14*, 1082; b) R. Neugebauer, T. Hipke, *Adv. Eng. Mater.* **2006**, *8*, 858.
[3] a) P. Schäffler, G. Hanko, H. Mitterer, P. Zach, presented at *Alulight Metal Foam Products", presented at Porous Metals and Metallic Foams: Metfoam*, Kyoto, Japan, September **2007**; b) F. García-Moreno, *Materials* **2016**, *9*, 85.
[4] a) A. R. Kennedy, *Powder Metall.* **2002**, *45*, 75; b) S. Asavavisithchai, A. R. Kennedy, *Adv. Eng. Mater.* **2006**, *8*, 810; c) H. M. Helwig, S. Hiller, F. Garcia-Moreno, J. Banhart, *Metall. Mater. Trans. B* **2009**, *40*, 755.
[5] I. Duarte, J. Banhart, *Acta Mater.* **2000**, *48*, 2349.
[6] a) F. Garcia-Moreno, J. Banhart, M. Haesche, K. Vignodhar, J. Weise, presented at *Cellular Metals for Structural and Functional Applications: CellMet*, Dresden, May **2005**; b) I. Duarte, M. Oliveira, F. Garcia-Moreno, M. Mukherjee, J. Banhart, *Colloids Surf., A* **2013**, *438*, 47.
[7] H. M. Helwig, F. Garcia-Moreno, J. Banhart, *J. Mater. Sci.* **2011**, *46*, 5227.
[8] D. Lehmhus, M. Busse, *Adv. Eng. Mater.* **2004**, *6*, 391.
[9] a) B. Matijasevic-Lux, J. Banhart, S. Fiechter, O. Görke, N. Wanderka, *Acta Mater.* **2006**, *54*, 1887; b) A. R. Kennedy, *Scripta Mater.* **2002**, *47*, 763; c) P. H. Kamm, F. García-Moreno, C. Jiménez, J. Banhart, *J. Mater. Res.* **2013**, *28*, 2436; d) X. Li, Y. Liu, J. Ye, X. An, Z. Cao, X. Liu, *Mater. Lett.* **2018**, *210*, 350.
[10] D. Lehmhus, G. Rausch, *Adv. Eng. Mater.* **2004**, *6*, 313.
[11] a) T. Neu, B. Pfretzschner, F. García-Moreno, J. Banhart, *Metals* **2017**, *7*, 323; b) D. Puspitasari, F. Khairullah Hishyam Rabie, T. Lenggo Ginta, J. Kurnia, M. Mustapha, *MATEC Web Conf.* **2018**, *225*, 01006.
[12] P. H. Kamm, F. García-Moreno, T. R. Neu, K. Heim, R. Mokso, J. Banhart, *Adv. Eng. Mater.* **2017**, *19*, 1600550.
[13] P. H. Kamm, T. R. Neu, F. García-Moreno, J. Banhart, *Acta Mater.* **2021**, *206*, 116583.
[14] I. Duarte, J. Mascarenhas, A. Ferreira, J. Banhart, *Adv. Mater. Forum I* **2002**, *230–2*, 96.
[15] F. Garcia-Moreno, N. Babcsan, J. Banhart, *Colloids Surf., A* **2005**, *263*, 290.
[16] F. Simancik, K. Behulova, L. Bors, presented at *Cellular Metals and Metal Foaming Technology: Metfoam*, Bremen, June **2001**.
[17] a) F. Garcia-Moreno, M. Mukherjee, C. Jiménez, A. Rack, J. Banhart, *Metals* **2011**, *2*, 10; b) F. Simancik, N. Minarikova, S. Culak, J. Kovacik, presented at *Metfoam 1999*, Bremen, June **1999**.
[18] C. Körner, F. Berger, M. Arnold, C. Stadelmann, R. F. Singer, *Mater. Sci. Technol.* **2000**, *16*, 781.
[19] a) F. Garcia-Moreno, N. Babcsán, J. Banhart, presented at Metfoam, Kyoto, Japan, September 2005; b) G. S. Vinod Kumar, M. Mukherjee, F. Garcia-Moreno, J. Banhart, *Metall. Mater. Trans. A* **2013**, *44*, 419; c) Z. K. Cao, Y. Yu, M. Li, *Mater. Sci. Forum* **2018**, *933*, 106.
[20] F. Garcia-Moreno, M. Mukherjee, C. Jiménez, J. Banhart, *JOM* **2015**, *67*, 955.
[21] H. Stanzick, I. Duarte, J. Banhart, *Materialwiss. Werkstofftech.* **2000**, *31*, 409.
[22] C. Okolieocha, D. Raps, K. Subramaniam, V. Altstädt, *Eur. Polym. J.* **2015**, *73*, 500.
[23] F. Garcia-Moreno, M. Fromme, J. Banhart, *Adv. Eng. Mater.* **2004**, *6*, 416.
[24] a) J. Banhart, *Advanced Tomographic Methods in Materials Research and Engineering* (Ed: R. J. Brook), Oxford University Press, Oxford **2008**, pp. 462; b) M. Saadatfar, F. Garcia-Moreno,

S. Hutzler, A. P. Sheppard, M. A. Knackstedt, J. Banhart, D. Weaire, *Colloids Surf A-Physicochem. Eng. Asp.* **2009**, *344*, 107.
[25] C. Jiménez, F. Garcia-Moreno, B. Pfretzschner, M. Klaus, M. Wollgarten, I. Zizak, G. Schumacher, M. Tovar, J. Banhart, *Acta Mater.* **2011**, *59*, 6318.
[26] M. Mukherjee, F. Garcia-Moreno, J. Banhart, *Acta Mater.* **2010**, *58*, 6358.
[27] V. Vanessa, in *Fachgebiet Struktur und Eigenschaften von Materialien des Instituts für Werkstoffwissenschaften und -technologien der Technischen Universität Berlin, Bachelor Thesis*, Technische Universität Berlin, Berlin **2018**.
[28] B. Matijasevic, J. Banhart, *Scr. Mater.* **2006**, *54*, 503.
[29] E. Andrews, W. Sanders, L. J. Gibson, *Mater. Sci. Eng., A* **1999**, *270*, 113.
[30] a) J. L. Grenestedt, *J. Mater. Sci.* **2005**, *40*, 5853; b) U. Ramamurty, A. Paul, *Acta Mater.* **2004**, *52*, 869.
[31] A. Rack, H. M. Helwig, A. Bütow, A. Rueda, B. Matijašević-Lux, L. Helfen, J. Goebbels, J. Banhart, *Acta Mater.* **2009**, *57*, 4809.
[32] F. García-Moreno, M. Jürgens, J. Banhart, *Acta Mater.* **2020**, *196*, 325.
[33] C. Körner, M. Thies, R. F. Singer, *Adv. Eng. Mater.* **2002**, *4*, 765.
[34] F. Garcia-Moreno, E. Solorzano, J. Banhart, *Soft Matter* **2011**, *7*, 9216.
[35] M. Mukherjee, F. Garcia-Moreno, J. Banhart, *Metall. Mater. Trans. B* **2010**, *41*, 500.
[36] J. Campbell, *Castings: The New Metallurgy of Cast Metals* (Ed: J. Campbell), Butterworth-Heinemann, Oxford, UK **2003**.